*Journal of Applied Fluid Mechanics*, Vol. 12, No. 6, pp. 1745-1755, 2019.
Available online at www.jafmonline.net, ISSN 1735-3572, EISSN 1735-3645.
DOI: 10.29252/jafm.12.06.29685

# Turbulence Model Selection for Heavy Gases Dispersion Modeling in Topographically Complex Area

Fz. Mirzaei[1], Fs. Mirzaei[1] and E. Kashi[2†]

[1] *Energy Department, Politecnico di Milano, Italy*
[2] *Department of Chemical Technologies, Iranian Research Organization for Science and Technology (IROST), Tehran, Iran*

†*Corresponding Author Email: kashi@irost.ir*

(Received October 3, 2018; accepted March 2, 2019)

## ABSTRACT

The dispersion of hazardous gas in the environment presents dangerous risks for people living close to chemical plants or storages. Since heavy gases tend to stay at lower levels and disperse at a slower pace in the atmosphere, they are potentially more dangerous. In this paper, various mathematical models for turbulence (including k-ε, RNG k-ε, EARSM, LES, DES) and their associated parameters have been assessed, compared and validated against the experimental data in various scenarios to find the most suitable one for atmospheric dispersion of dense-gases. This topic has been investigated and validated by a computational fluid dynamics (CFD) simulation of the Kit-Fox experiment. The precision of the CAD models, practicality, computational resource requirements, and some other factors have been considered and addressed in this paper to achieve a comprehensive solution for atmospheric dispersion. The results here suggest that the proper selection of the turbulence model and the turbulent Schmidt number is crucial. Our results indicate that the most promising combination in the case of atmospheric dense-gas dispersion is the RNG k-ε model with the Schmidt number of 0.4, considering the demand for accuracy and computational resource.

**Keywords:** Turbulence modeling; Computational Fluid Dynamics; EARSM; RNG k-ε model; Atmospheric dispersion.

## 1. INTRODUCTION

The possible release, leakage and dispersion of hazardous gases into the atmosphere resulting from human errors, terrorist attacks, mechanical failures, etc. could potentially endanger the life and well-being of the people living nearby. Common atmospheric gas dispersion models (e.g. HEGADAS, ALOHA®, CALPUFF, etc.) have been developed and evaluated using field and wind tunnel data (Hanna and Chang, 2001; Hanna and Britter, 2002; Hanna *et al*., 2008). In these models, the surface roughness is the only parameter that considers the presence of physical obstacles, and it is used to modify and correct the wind profile solely. However, in recent years, the use of the CFD approach in modeling gas dispersion scenarios has been more common as computers are becoming faster and more capable. Meanwhile, CFD codes provide more accurate results in comparison to traditional gas dispersion models (Tominaga & Stathopoulos 2007; Kashi *et al*. 2015a; Gavelli *et al*. 2008; Giannissi *et al*. 2015).

General-purpose CFD packages such as ANSYS CFX® and ANSYS Fluent® have been available for many years for modeling various types of flows in three dimension (3D) (ANSYS Inc, 2016a), alongside open-source solutions like OpenFOAM®. These codes have been successfully applied and validated for problems associated with reaction engineering, solid mechanics, wind effects and gas flows (Gavelli, Bullister and Kytomaa, 2008). CFD predictions are usually validated with suitable experimental data. The CFD methods are more attractive in comparison to wind-tunnel experiments since they can deliver results faster, cheaper, and safer. An important parameter which can greatly affects the results of CFD simulations is the choice of the appropriate turbulence model and its associated parameters (Tominaga and Stathopoulos, 2007; Karthik, 2011; Zhu *et al*., 2013).

Numerical simulations of atmospheric gas dispersion with the ANSYS CFX® platform have been investigated for both isolated cubes obstacles and arrays of obstacles by Kashi *et al*. (2009). As a case in point, the Thorney Island and the Kit-Fox experiments have been used for validating their methodologies. The turbulence model used in the mentioned paper was the two-equation standard k-ε, which has been commonly used by many researchers (Hoi *et al*., 2006; Gavelli, Bullister and Kytomaa,

2008). The CFD method can be used for large-scale gas dispersion simulations on a city scale, which are analogous to the Kit-Fox experimental works that consider cubical obstacles like buildings and other barriers as the arrays of obstacles in a city (Kashi *et al*. 2015b). It has been stated in various research papers (Hu *et al*., 2011; Tominaga and Guo-cheng, 2012) that gas dispersion simulations in a complex environment are similarly feasible and very effective with ANSYS CFX® codes. Furthermore, the relevant software is crucial to define the problem correctly and precisely at the beginning of the simulation along with the use of accurate CAD models, sufficient mesh quality, setting proper boundary layers, choosing the best turbulence model, and setting correct parameters for achieving more accurate results (Amorim *et al*. 2013; Katz & Sankaran 2011; Tominaga & Stathopoulos 2013; Kashi *et al*. 2015a; Hoi *et al*. 2006).

In this paper, various relevant turbulence models and their associated parameters are investigated to find the most suitable one for atmospheric dispersion of dense-gases. Models such as k–ω and some others have not been considered as they have already been assessed for these conditions and scenarios (Yu and The, 2016).

## 2. TURBULENCE MODELS

Turbulence modeling is the creation of a mathematical model to estimate and predict the effects of turbulence phenomena. To clarify, turbulent flow has some characteristics on various length scales. Typically, this methodology is the time-average of the governing equations, allowing for the focus on the large-scale and non-fluctuating characteristics of the fluid flow. Nevertheless, the properties and impacts of some small scales and fluctuating parts must be taken into consideration (ANSYS Inc, 2016a).

### 2.1 Standard k-ε

The standard k-ε is the most commonly used and well-known turbulence model. This model has been used by many authors for the application of atmospheric dispersion. (Sklavounos & Rigas 2004; Tominaga & Guo-cheng 2012; Gavelli *et al*. 2008; Kashi *et al*. 2015a) It is a two-equation model from the Reynolds-averaged Navier-Stokes (RANS) group, where the first transported variable is turbulent kinetic energy, *k*, and the second transported variable is turbulent dissipation, ε. The ε equation governs the scale of the turbulence, and the *k* equation describes the energy in the turbulence.

### 2.2 RNG k-ε Model

In the RNG k- ε model, the k-ε equations are derived from the application of a statistical technique (Re-Normalization Group Method) to the instantaneous Navier-Stokes equations. This model was developed by Yakhot *et al*. (1992) to re-normalize the original Navier-Stokes equations to account for the impacts of smaller scales of motion flows.

The RNG k-ε model is based on the standard k-ε equations, but it also includes the following features:

- The extra term in the ε equation to account for the interaction between turbulence dissipation and the mean shear.
- A differential equation for the effective viscosity.
- The occurrence of a swirling effect on the turbulence.
- The formula for turbulent Prandtl number (Viscous diffusion rate/Thermal diffusion rate).

Some improvements in the predictions for the high streamline curvature, transitional flows, and separated flows are suggested. Moreover, the time-dependent flows with large-scale motions are better predicted.

### 2.3 Explicit Algebraic Reynolds Stress Models (EARSM)

The Explicit Algebraic Reynolds Stress Models (EARSM) represent the extended forms of the standard two-equation turbulence models (e.g. k-ε, k-ω, etc.). These models are derived from the Reynolds stress transport equations; they consider a nonlinear relation between the Reynolds stress terms, $R_{ij,}$ and the mean strain-rate and vorticity tensors present in the flow field. These types of models are a simplified form of the Reynolds stress models (RSMs) and are mostly used in problems with secondary flows as well as flows with streamline curvature (i.e. swirling flow) (Wallin and Johansson 2000; ANSYS Inc, 2016b).

The nonlinear equations suggested by Wallin *et al*. for the Reynolds stresses characterizes an extension over the *linear Boussinesq hypothesis* (Wallin & Johansson 2000). As a result of using this hypothesis, these models are known as nonlinear eddy viscosity models as opposed to linear eddy viscosity models (e.g. Standard k-ε) (Wallin and Johansson 2000).

### 2.4 Large Eddy Simulation (LES)

Usually, the size of the computational domain should be at least an order of magnitude greater than the scales describing the turbulence energy, while the mesh must be fine enough to resolve the smallest dynamically significant length scale (the Kolmogorov micro-scale) for precise simulation. The most precise method for the simulation of turbulent flows is direct numerical simulation (DNS) in which the full Navier–Stokes equations are numerically solved using very fine mesh. Consequently, DNS is a computationally more demanding method and currently, it can only be used for low Reynolds number flows over simple geometry. This is the base for the RANS method in which only the averaged quantities are implemented while the effect of all the scales of instantaneous turbulent motion is modeled by a turbulence model. However, sometimes the RANS method fails to predict some of the flow behavior such as the transient flow (Zhiyin, 2015).

As an alternative, large-eddy simulation (LES) was introduced in as early as 1963 by Smagorinsky. LES does not use conventional averaging like the RANS method with the added modeled transport equations being solved to get the so-called Reynolds stresses resulting from the averaging process. In LES, large eddies are computed directly and only sub-grid scale (SGS) motions are modeled, resulting in a substantial drop in computational cost compared to DNS. LES tends to be more precise than the RANS method since the large eddies hold most of the turbulent energy and are responsible for most of the momentum transfer and turbulent mixing. LES captures these eddies in full detail; however, they are modeled in the RANS method. Moreover, the small scales tend to be more isotropic and homogeneous than the large ones, and thus, modeling the SGS motions would be easier than modeling all scales within a single model as in the RANS method. Thus, LES is currently the most promising numerical tool for simulating realistic turbulent flows.

### 2.5 Detached Eddy Simulation (DES)

Detached eddy simulation (DES) is a variation of a RANS model where the model shifts to a sub-grid scale formulation in sections fine enough for the LES model. The regions near the solid boundaries and where the turbulent length scale are less than the maximum grid dimension is allocated the RANS method of solution. As the turbulent length scale exceeds the grid dimension, the regions are solved using the LES method. Consequently, the grid resolution is not as demanding as the pure LES, thus significantly reducing the computational demand. Although DES was initially formulated for the Spalart-Allmaras model, it can be applied to other RANS models by properly adjusting the length scale, which is explicitly or implicitly involved in the RANS model. Subsequently, while the Spalart-Allmaras model that is based on DES acts as a LES with a wall model, the DES that is based on other models (like two-equation models) behave as a hybrid RANS-LES model. The grid generation is more complex than that of a simple RANS or LES case due to the RANS-LES switch. DES is a non-zonal method and delivers a single smooth velocity field across the RANS and the LES regions of the solution (Center, 2012).

## 3. Validation Of The CFD Code

To be able to validate the methodology and codes, it is necessary to compare the results against precise experimental data. For this purpose, the Kit-Fox experiment has been chosen, as it is one of the most respectful experimental works in the gas dispersion analysis field. (Hanna and Chang, 2001)

### 3.1 Kit-Fox Experiments and its Test Site Details

Dense-gas dispersion experiments, also known as the Kit-Fox experiments, were conducted in August of 1995 at the "Frenchman Flat" area of the Nevada National Security Test Site, under the support of U.S. Environmental Protection Agency (EPA) and the U.S. Department of Energy. This American nuclear test site is located North-West of Las Vegas and has a 15 $km^2$ dry lake bed. The "Frenchman Flat" is located within area 5 of the Nevada test site and can be observed in Figure 1. These experiments were meant to simulate gas dispersion scenarios in an industrial site scaled at 1/10 of the actual size. The main objective of this research was to study the dense-gas dispersion over rough surfaces and under stable ambient conditions.

The "HEGADAS*"* gas dispersion model was used to help design the placement of $CO_2$ sensors and climatic sensors in the Kit-Fox experiment. The code results were also used to plan the $CO_2$ release rates so that the anticipated dense gas effects could be sensed with the least amount of gas releases. The HEGADAS results for the concentrations, cloud height and cloud width were generated for a variety of scenarios, atmospheric inputs, and surface roughness's ($z_0$) to propose the calibration ranges for the sensors and their specific locations in the space. The lateral spacing of the sensors (near 6 meters on the closest arc and about 10 meters on the farthest arc) and their maximum heights (near 5 meters on the closest arc and about 10m on the farthest arc) on the 9 towers were likely to capture the cloud, which were based on these HEGADAS results (Hanna and Chang, 2001). In Table 1, examples of additional information available for each trail can be observed.

**Table 1 Additional Information on Trial 3 Release Number 7**

| Trial ID | KF0307 |
|---|---|
| Source Exit pressure (atm) | 0.8928 |
| Source Temperature (K) | 298.4 |
| Roughness Length $z_0$ (m) | 0.12 |
| Friction Velocity u* (m/s) | 0.21 |
| Bowen Ratio Estimate | -99.9 |
| Inverse Monin-Obukhov length (1/m) | 0.05882 |
| Total released (kg) | 72.94 |
| Initial concentration (ppm) | 995700 |
| Ambient Pressure (atm) | 0.8928 |
| Relative Humidity (%) | 5 |

During this series of experiments, $CO_2$ (the dense-gas) was released for 2 to 5-minute periods (representing continuous plumes) and 20-second periods (representing short-duration transient puffs) under the Pasquill-Gifford stability classification of "F" (stable ambient conditions). The desert surface was artificially roughened by the blending of obstacles in order to simulate the roughness of a typical industrial area.

According to Hanna and Chang (Hanna and Chang, 2001), in the Kit-Fox experiments, a total of 52 gas release trails collected in 7 days were considered more accurate than the others. Therefore, we have chosen our simulations from these releases in order to have better and more precise simulations. These candidate trails are presented in Table 2.

Figure 2 demonstrates the plot plan of the test site,

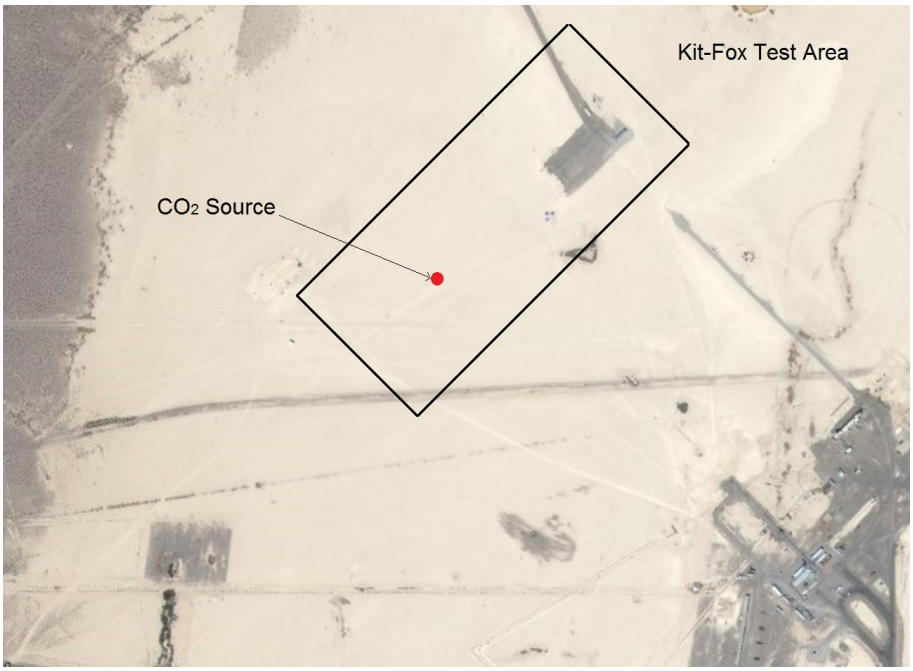


**Fig. 1. Kit-Fox experiment location and $CO_2$ Source, Acquired from Bing® Maps by Microsoft.**

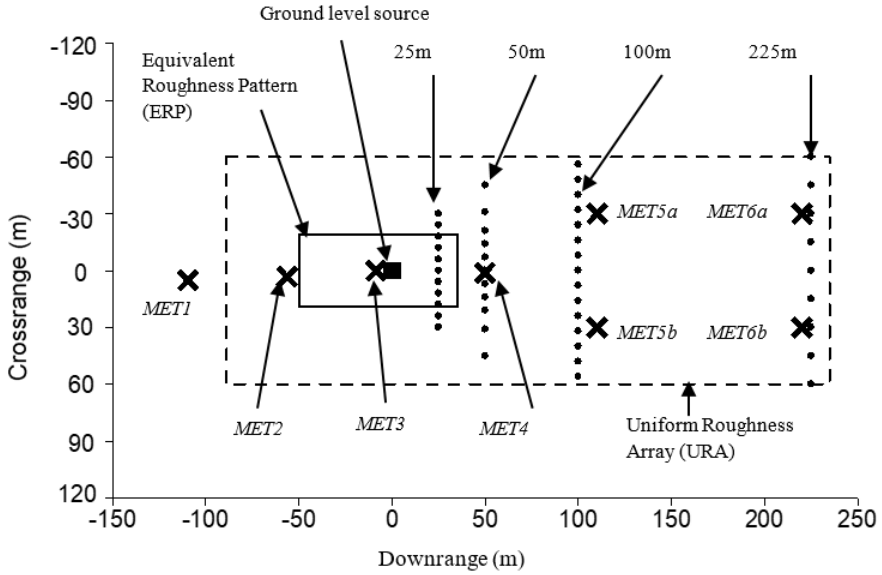


**Fig. 2. Plot plane of the Kit-Fox Test Site.**

where a local Cartesian coordinate system as defined by the Western Research Institute (WRI) is used.

## 3.2 Boundary Conditions

### 3.2.1 Wind Profile Model and Surface Roughness

Due to the existence of the actual wind data, to achieve more accurate results, no correlation has been used to find the wind profile in this simulation. The provided meteorological data (from Kit-Fox datasets) were directly applied as the wind inlet profile at the boundaries. By using this method, one can carefully define the wind speed and its direction at any time and in any height.

### 3.2.2 Gas Emission Source

As suggested by Hanna and Chang, the 7$^{th}$ release of the 3$^{rd}$ trial of the Kit Fox field experiment was considered to be a more accurate experiment in comparison to the others (Hanna and Chang, 2001). During this part of the experiment, $CO_2$ gas was released instantly into the atmosphere at the rate of 3.65 kg/s and for the duration of 20 seconds. This was implemented in the CFX® code as a step function:

$$Q_i = m_i(step[t] - step[t-20]) \quad (1)$$

The mass flow rate of the $CO_2$ gas from the source location was specified. In order to have fully developed flows in the simulations, the initial time-

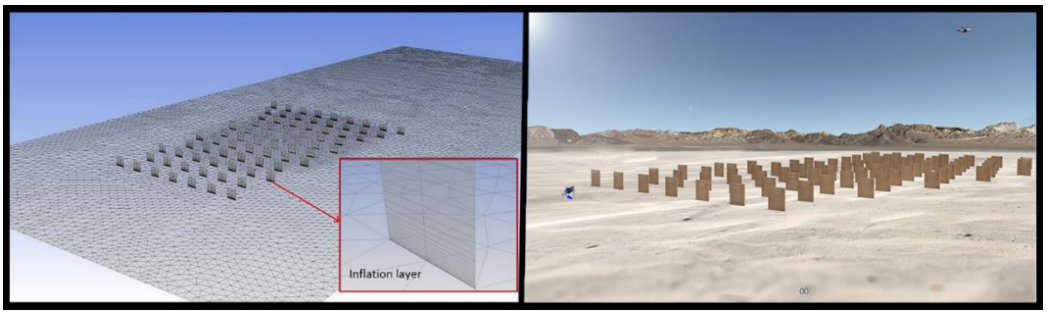


**Fig. 3. Model Structure and Level of Details for the Kit-Fox experiment site.**

step of the gas release was considered to occur 50 seconds after the start of the simulation. Since the gas source was at ground level, and during the experiment, the ground surface temperature was around 29°C; the initial gas temperature was set to 29°C in the simulations. The temperature was used by the code to calculate the thermodynamic behavior of the gas.

**Table 2 Candidates of Gas Release Experiments**

| Date of the Experiment | Trail Number | Number of Releases |
|---|---|---|
| 08/24/1995 | 2 | 2 |
| 08/25/1995 | 3 | 7 |
| 08/26/1995 | 4 | 2 |
| 08/28/1995 | 5 | 8 |
| 08/29/1995 | 6 | 9 |
| 08/30/1995 | 7 | 12 |
| 08/31/1995 | 8 | 12 |

Furthermore, all the important initial conditions (IC) and boundary conditions (BC) were taken into account in the CFD simulations. To speed-up the simulations and reducing the computational time, a combination of 2D and 3D geometry was used for the validation. The details of the simulation settings are presented in Table 3.

### 3.2.3 Mesh Verification

The robustness of the mesh has been studied intensely for the same experiment in our previous publication (Kashi *et al*. 2015a). For discretization purpose, second-order scheme is used. When second-order accuracy is chosen, quantities at cell faces are computed using a multidimensional linear reconstruction approach. In this approach, higher-order accuracy is reached at cell faces through a Taylor series expansion of the cell-centered solution about the cell centroid. Grid convergence study has been performed from an initial coarse mesh, followed by a more refined mesh through a 1.5 factor and a fine grid level with a factor of 2.0. Surface mesh quality and T-rex wall boundary initial spacing has been checked thoroughly for each level of the grid before choosing the best one.

In Figure 3, the level of detail (LOD) and mesh quality of the area model is presented.

## 4. Results And Discussion

To find the best turbulence model and parameters for the simulations, the simulation was run with various parameters and turbulence models which were compared to the experimental data from various sensors in the field (here, Trial 3 and the release number 7 of the Kit-Fox experiment). For this purpose, the Standard k-ε, EARSM, RGN k-ε, Detached Eddy Simulation (DES) and LES (Large Eddy Simulation) turbulence models were considered.

As suggested by Tominaga and Stathopoulos, the Schmidt number can varies between 0.2 and 1.3 (Tominaga and Stathopoulos, 2007). Nevertheless, it is worth noting that although the Schmidt number had an impact on the results, the impact on the sum of the squared residuals (SSR) between the Schmidt number of 0.4 and 0.7 for the RNG k-ε turbulence model was not as huge as was expected. Consequently, on the basis of the lowest SSR, the Schmidt number was considered to be 0.4 for all the scenarios as it was also suggested by some authors (Tominaga and Stathopoulos, 2007).

The following sensors have been considered and compared to the experimental results: P1002, P1003, P1132, P2001, P2003, P2004, P2111 and P3001 in trial 3 and the release number 7 of the Kit-Fox experiment (Table 4).

The k-ε model has been chosen as the starting base turbulence model; it is a commonly used model in these types of simulations to carry out the comparison against the experimental data.

### 4.1 Impact of Some Parameters on the Results

#### 4.1.1 Impact of the Humidity

According to the results of the experiments and simulations of Hongya Zhu *et al*. (2013), the parameter of humidity almost has no tangible impact on the methane flammable vapor cloud dispersion distance. (Zhu *et al*., 2013) Meanwhile, our own simulations demonstrate comparable results for the case of carbon dioxide ($CO_2$) dispersion. The addition of humidity to the environment shows *a negligible impact* on the results in all our cases. Correspondingly, adding humidity ($H_2O$ vapor) in the environment did not add a significant

**Table 3 Simulations configuration and Details**

| Parameter | Value |
|---|---|
| CFD Code | ANSYS CFX R18 |
| Number of Elements (nodes) | 1.72 M (0.52 M) |
| Mesh (Quality, Expansion rate, Skewness) | 0.5, 5, 0.7 |
| Composition | Air and $CO_2$ at STP Conditions |
| Morphology | Continues Fluid Morphology |
| Reference Pressure (absolute) | 1 atm |
| Buoyancy Turbulence | Production and Dissipation (Turbulence Schmidt number 0.4 is chosen) |
| Domain Motion | Stationary |
| Heat Transfer Phenomena | Not Considered (Homogeneous Model) |
| Turbulence model | k- ε, RNG k-ε, EARSM, DES, LES |
| Wall Function | Scalable Wall Function |
| Wind (Inlets) in 2 boundaries | Turbulence option is high (intensity 10%) in one and the turbulence option is medium in the other |
| Other boundaries (3 others) | Considered as opening as boundary type with the medium turbulence option of the intensity of 5% |
| Ground surface (boundary) | Considered as boundary type of the wall with the sand grain surface roughness of 0.01 [m] |

computational load on our simulations, the impact is in the order of less than a 1 percent increase on the computational time.

**Table 4 Tag Names and Locations of Nova Sensors in Downwind Arrays**

| Sensor Details | | Location (Cartesian Coordinate) | | |
|---|---|---|---|---|
| Tag Name | Range (ppm) | Y (m) | X (m) | Z (m) |
| P1002 | 0-50k | 0 | 25 | 0.6 |
| P1003 | 0-50k | 0 | 25 | 1.2 |
| P1132 | 0-50k | 12 | 25 | 0.6 |
| P2001 | 0-50k | 0 | 50 | 0.5 |
| P2003 | 0-10k | 0 | 50 | 2 |
| P2004 | 0-10k | 0 | 50 | 4 |
| P2111 | 0-50k | 7 | 50 | 0.6 |
| P3001 | 0-10k | 0 | 100 | 0.6 |

### 4.1.2 Impact of the Turbulent Schmidt Number

According to Bergman *et al*., the turbulent Schmidt number is a dimensionless number defined as the ratio between the rates of turbulent transport of momentum and the turbulent mass transport rate (Bergman *et al*., 2011). It is analogous to the turbulent Prandtl number, which deals with turbulent heat transfer as opposed to the turbulent mass transfer rate.

$$Sc_t = \frac{v_t}{\mathrm{K}} \tag{2}$$

Equation 2 illustrates the turbulent Schmidt number as the ratio of *eddy viscosity* $v_t$ ($m^2/s$) over *eddy diffusivity* K ($m^2/s$). In CFD, when we are using Reynolds-averaged Navier–Stokes equations to model turbulent flows, the mass transfer usually is estimated by the turbulent scalar flux (assuming the gradient diffusion), which needs the definition of the turbulent Schmidt number prior to the calculation. As for the atmospheric dispersion, this number is usually suggested to range between 0.2-1.3 (Tominaga and Stathopoulos, 2007). However, this is a rather wide range and more specific values are needed for atmospheric gas dispersion. Tominaga *et al*. suggested that the Schmidt number must be defined within this range by considering the dominant flow in each case (Tominaga and Stathopoulos, 2007). Other authors have suggested narrower ranges and in some cases, a specific value for the Schmidt number (Tominaga and Guo-cheng, 2012; Giannissi, Venetsanos and Markatos, 2015; Yu and The, 2016). To demonstrate these variations, different Schmidt values used by different authors are listed in Table 5.

**Table 5 Various Turbulent Schmidt Number Used in Atmospheric Dispersion**

| Turbulent Schmidt Number | Author, Year |
|---|---|
| 0.2-0.7 | (Yu and The, 2016) |
| 0.3-0.7 | (Gousseau *et al*., 2011) |
| 0.40 | (Nakibouglu *et al*., 2009) |
| 0.63 | (Lien *et al*., 2006) |
| 0.70 | (Li and Stathopoulos, 1997; Vardoulakis and Cai, 2011; Mokhtarzadeh-dehghan, Akcayoglu and Robins, 2012) |
| 0.72 | (Giannissi, Venetsanos and Markatos, 2015) |
| 0.90 | (Delaunay, 1996; Kim and Baik, 2003; Santiago, Martilli and Martilli, 2007; Baik, Park and Kim, 2009) |
| 1.00 | (Antonioni *et al*. 2012; Kashi *et al*. 2015a) |
| 0.7-1.4 | (Yang and Zhang, 2017) |

In this study, a sensitivity analysis has been done to find the most suitable Schmidt number. In order to do so, a gas dispersion case from the Kit-Fox experiences has been evaluated through the variation of the Schmidt number using the RNG k-ε turbulence model (the reason for selecting the RNG k-ε model

is explained later in this paper). Afterward, by considering the relative errors and using the SSR method (Sum of Squared Residuals), the most appealing Schmidt number has been selected for further analysis. The results can be found in Table 6 (only data from one sensor is provided in Table 6, as the rest of the sensors showed quite similar trends, and it is only provided for comparison purposes here). The SSR or the summation of the squared residual is calculated from the following equation:

$$SSR = \sum (\text{Experimental data} - \text{Model Prediction})^2 \quad (3)$$

**Table 6 Comparison of Different Schmidt Number in Kit-Fox Experiment using RNG k-ε for P1132 Sensor data**

| Schmidt Number | SSR |
|---|---|
| 0.2 | 3.14E+08 |
| 0.4 | 2.96E+08 |
| 0.7 | 3.04E+08 |
| 1.0 | 4.83E+08 |
| 1.2 | 5.39E+08 |

The difference between the SSR values becomes much less apparent when it is applied to the standard k-ε model. Overall, the most promising value for the Schmidt number here would be 0.4 as it has the lowest SSR, which is on par with other authors' suggestions. Overall, the optimal values for the Schmidt number depend on the local flow characteristics. Consequently, it is recommended that the Schmidt number should be found by considering the dominant flow behavior in each case-study (Tominaga and Stathopoulos, 2007). Consequently, the best Schmidt number for the case in hand would be the one with the lowest SSR value. In the case of not having the proper datasets for investigating the SSR values, the Schmidt number of 0.4 could be used as a rule of thumb for similar environmental gas dispersion.

### 4.1.3 CPU-Time and Hardware

The computation requirement varies in different models (Standard k-ε < RNG k-ε < EARSM < DES <LES). The parallel computation was performed on two WS laptops (Intel® Core™ i7-4720HQ) through Intel® distributed MPI. The total memory on both WS were 64 Gb. As an example, the standard k-ε setup took around 8 hours to converge to $10^{-4}$ in RMS, whereas the LES setup took around 120 hours to converge to $10^{-4}$ in RMS.

## 4.2 Results of the k-ε Model

The simulation results of the k-ε model are presented in Figures 4 to 8. In Figure 4, the turbulence model grasps the peak point of the concentration rather well but fails to match the trend before and after the peak point. In Figure 5, it can be seen that the simulation better matches the experimental results, however, the max concentration has more overshoot. In Figures 6 and 8, the turbulence model shows an acceptable match to the experimental data up until the point that they went to zero and fail to grasp the trend until the end of the time period. Figure 7 demonstrates the fluctuations in the results of the simulations in a rather strange manner. It is worth mentioning here that the model simulates the gas behavior better at higher heights (look at the results from the P1002 at 0.6m and P1003 at 1.2m), and it seems that the model fails to grasp the gas fluctuations close to the ground at lower concentrations. This behavior needs more investigation through experimental works to find the best heights for the location of the sensors in these types of works. Nevertheless, in general, the simulation results show an acceptable match to the experimental data.

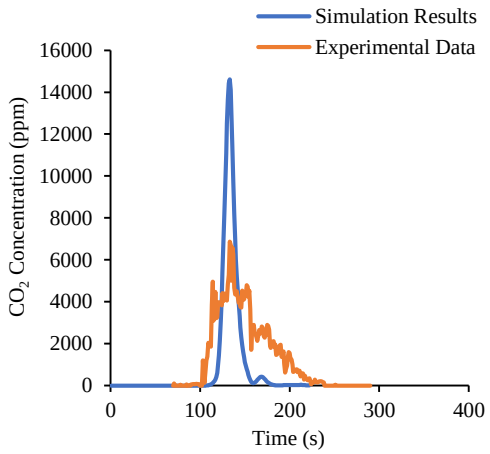


**Fig. 4. Sensor P1002 - k-ε Model vs. Experimental Data.**

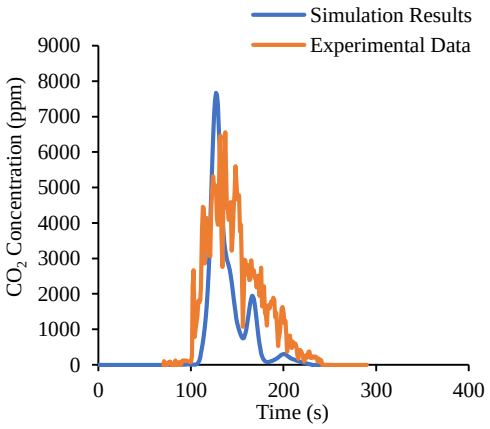


**Fig. 5. Sensor P1003 - k-ε Model vs. Experimental Data.**

## 4.3 Results of RNG k-ε Model

The turbulence model in Figure 9 shows a better match of the concentration in comparison to the standard k-ε model, but then again, it fails to fully match the trend before and after the peak point. Figure 10 also demonstrates a better outcome in comparison to the standard k-ε model. It is seen that on the P1132 sensor, it fails to match the experimental data until the end of the time period of

the simulation and goes to zero after 220 seconds. In Figure 11, the RNG k-ε turbulence model illustrates better results versus the standard k-ε model, despite the rather severe fluctuation of the concentrations. In general, the RNG k-ε model demonstrates significant lower deviation and error against the experimental data when compared to the simple k-ε model. It is worth noting that the impact of the RNG k-ε model on the computational time was just around a 15 to 20% increase when compared to the standard k-ε model. Once again, it is worth mentioning the fact that the model shows better results here again at higher heights (0.6m vs 1.2m) similar to the k-ε case.

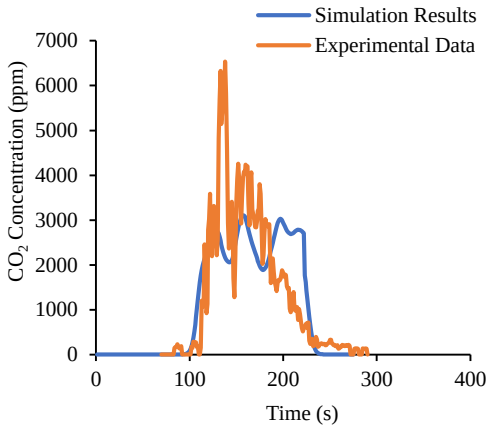


**Fig. 6. Sensor P1132- k-ε Model vs. Experimental Data.**

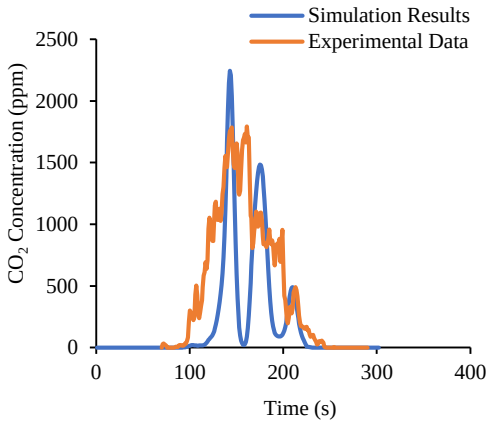


**Fig. 7. Sensor P2003- k-ε Model vs. Experimental Data.**

## 4.4 Comparison of all the Models

A comparison of the data from sensors P1002 and P1132 (Figures 4 and 6) demonstrates that the departure from the gas dispersion center-line would result in a worse match between the actual and simulated results. In other words, inside the wind direction, we would have a better prediction compared to the other regions. By examining the results from sensors P2003 and P2004 (Figure 11), we can see that the elevation level would not affect the data match in the far distances, whereas the results from the nearer sensors to the source, like P1002 and P1003 (Figure 4 and Figure 5), show that this effect is more pronounced in the nearfield regions with a lower elevation level. This suggests that the simulation is well suited in longitudinal directions, where the convective phenomenon is dominant but less favorable in the transversal directions (y, z) which are dominated by the conduction phenomenon.

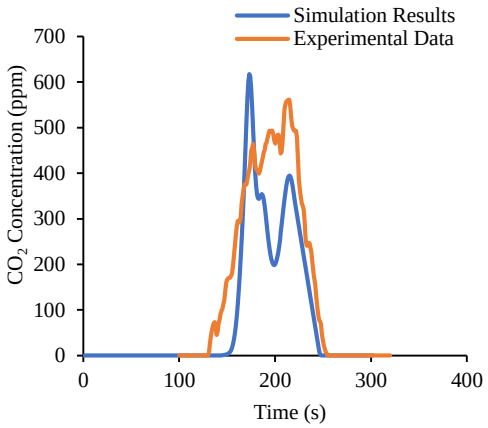


**Fig. 8. Sensor P3001- k-ε Model vs. Experimental Data.**

The results of the simple k-ε model are shown as the baseline, as it is used commonly by engineers. As the results of the EARSM were relatively close to those of RNG k-ε, presenting the figures for its sensors data seems to be redundant. The method of assessment is the comparison between the overall concentrations recorded by the sensors (Sum of all the concentration recorded by each sensor in our specific time-period). In Table 7, the overall relative errors between the simulation and the experimental data are shown. This has been done by comparing the actual data with the simulation results using Equation 3, where the objective function to be minimized is the overall sum of the squared residuals for each model and the experiment.

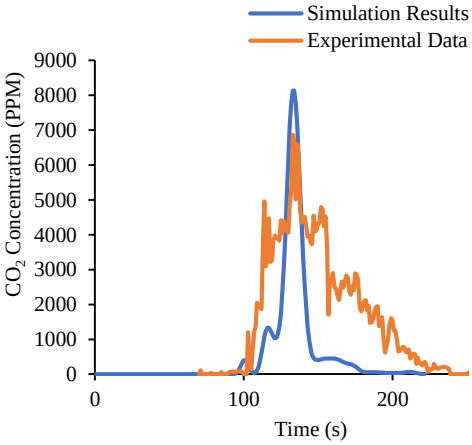


**Fig. 9. Sensor P1002 - RNG k-ε Model vs. Experimental Data.**

**Table 7 Overall concentration relative error of the simulation versus the experimental data.**

| Turbulence Model | P1002 | P1003 | P1132 | P2003 | P2004 | P3001 |
|---|---|---|---|---|---|---|
| RNG k-ε | 0.5938 | 0.4483 | 0.1137 | 0.3817 | 0.3667 | 0.3968 |
| Standard k-ε | 0.6371 | 0.4369 | 0.0695 | 0.466 | 0.4572 | 0.4385 |
| EARSM | 0.6452 | 0.4496 | 0.1263 | 0.4239 | 0.3846 | 0.3713 |
| DES | 0.9090 | 0.8899 | 0.7800 | 0.9909 | 0.7065 | 0.9992 |

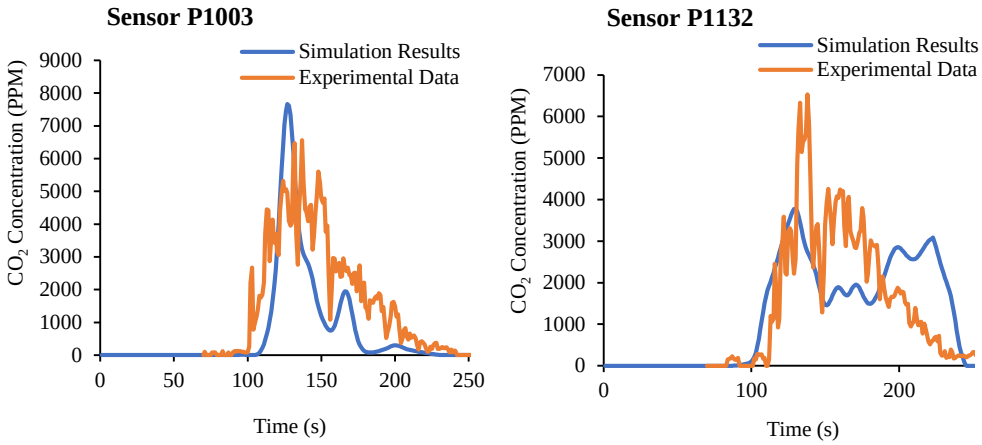


**Fig. 10. Sensor P1003 and P1132 - RNG k-ε Model vs. Experimental Data.**

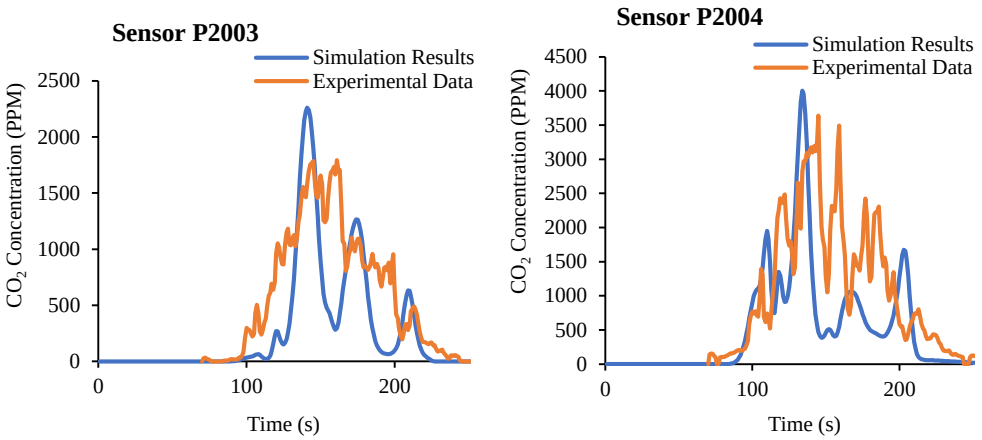


**Fig. 11. Sensor P2003 and P2004 - RNG k-ε Model vs. Experimental Data.**

In this comparison, it can be observed that the RNG k-ε model has the lowest overall concentration error when considering the errors from all the sensors. This is followed by the EARSM model, and the last one is the simple k-ε model. In general, the RNG k-ε model proved to be the best one in P1002, P2003, P2004, while the simple k-ε surprisingly showed a significantly lower error in P1132 in comparison to the others and slightly better than the others in P1003. The EARSM proved to be better only in the P3001. The reason for the dominance of RNG k-ε could be due to the extra term in the ε equation, which accounts for the interaction between turbulence dissipation and the means shear. It is important to mention that the computational demands and computational time of the EARSM were on par with the RNG k-ε model.

Another interesting outcome here is that all the models show significantly better results when the sensor is located at higher levels (0.6m vs. 1.2m); it appears that all these turbulence models grasp the gas behavior to a greater degree further from the ground level.

It is worth noting that the results from the Detached Eddy Simulation (DES) model were strongly inaccurate. Theoretically, these models were supposed to have better outcomes than the RANS models. The errors we observed here could have resulted from the escalation of numerical errors involving the solver's methods. Further investigation of similar models is required.

Simulations were also done using the LES (Large Eddy Simulation) turbulence model on a mesh with eight times more elements. Nonetheless, each simulation took weeks to converge, and our first few runs demonstrated unsatisfactory results with overall relative errors significantly higher than the rest. It

was decided that these types of simulations were not computationally feasible with our current available computational resources. Hence, spending time on debugging, analyzing and correcting the associated parameters seemed impossible. We expected the results from the LES to be more accurate than the rest, but our initial results were clearly not.

## 5. CONCLUSION

In this paper, the analysis of various turbulence models and their associated parameters were evaluated to find the most appropriate one for the atmospheric dispersion of dense-gases. This subject was addressed and validated through the simulation of Kit-Fox experimental works in ANSYS CFX® R18. The precision of the CAD models, practicality, computational resource requirements, and some other factors were all considered in this paper to achieve a comprehensive solution for heavy-gas dispersion in the atmosphere. It turned out that among the evaluated turbulence models, the outcomes of the RNG k-ε model with the Schmidt number of 0.4 proved to be the most accurate with relatively moderate computational resource demand. Furthermore, it was verified that all the turbulence models, which were tested during this study, demonstrated better results at distances further from the ground level. This was followed by the EARSM model, as it had the second-lowest overall sum of the squared residuals of the errors. By comparing the data, we concluded that the simulation was well suited in longitudinal directions, where the convective phenomenon was dominant but less favorable in the transversal directions (y, z) which were dominated by conduction phenomenon. Future works could address the impact of mesh quality on various turbulence models and maybe include the accurate data from more demanding models like the Large Eddy Simulation turbulence model.

## ACKNOWLEDGMENT

This research received no specific grant from any funding agency in the public, commercial, or not-for-profit sectors. The authors would like to thank Professor J. C. Chang and Professor S. Hanna for providing the Kit-Fox gas dispersion experiments data.

## REFERENCES

Amorim, J. H., V. Rodrigues, R. Tavares, J. Valente, and C. Borrego (2013). CFD modelling of the aerodynamic effect of trees on urban air pollution dispersion. *Science of the Total Environment* 461, 541–551.

*ANSYS Inc* (2016a) ANSYS CFX-Solver Theory Guide, Canonsburg, PA.

*ANSYS Inc* (2016b) ANSYS Fluent Theory Guide. Canonsburg, PA.

Antonioni, G., S. Burkhart, J. Burman, A. Dejoan, A. Fusco, R. Gaasbeek, T. Gjesdal, A. Jäppinen, K. Riikonen, P. Morra and O. Parmhed (2012). Comparison of CFD and operational dispersion models in an urban-like environment. *Atmospheric Environment* 47, 365–372.

Baik, J. J., S. B. Park and J. J. Kim (2009). Urban flow and dispersion simulation using a CFD model coupled to a mesoscale model. *Journal of Applied Meteorology and Climatology* 48(8), 1667–1681.

Bergman, T. L., F. P. Incropera, D. P. DeWitt and A.S. Lavine (2011). *Fundamentals of Heat and Mass Transfer*, Wiley.

Center, L. R. (2012). The Spalart-Allmaras Turbulence Model. In *Turbulence Modeling Resource* 1–9.

Delaunay, D. (1996). Numerical simulation of atmospheric dispersion in an urban site: Comparison with field data. *Journal of wind engineering and industrial aerodynamics* 64(2–3), 221–231.

Gavelli, F., E. Bullister and H. Kytomaa (2008). Application of CFD (Fluent) to LNG spills into geometrically complex environments. *Journal of Hazardous Materials* 159(1), 158–168.

Giannissi, S. G., A. G. Venetsanos and N. Markatos (2015). CFD Modeling of LNG Spill: Humidity Effect on Vapor Dispersion. *Journal of Physics: Conference Series* 633, 12136.

Gousseau, P., B. Blocken, T. Stathopoulos and G. J. F. Van Heijst (2011). CFD simulation of near-fi eld pollutant dispersion on a high-resolution grid : A case study by LES and RANS for a building group in downtown Montreal. *Atmospheric Environment* 45(2), 428–438.

Hanna, S., S. Dharmavaram, J. Zhang, I. Sykes, H. Witlox, S. Khajehnajafi and K. Koslan (2008). Comparison of six widely-used dense gas dispersion models for three recent chlorine railcar accidents. *Process Safety Progress* 27(3), 248–259.

Hanna, S. R. and R. E. Britter (2002). *Wind Flow and Vapor Cloud Dispersion at Industrial and Urban Sites*, John Wiley & Sons, 2010.

Hanna, S. R. and J. C. Chang (2001). Use of the Kit Fox field data to analyze dense gas dispersion modeling issues. *Atmospheric Environment* 35(13), 2231–2242.

Hoi, Y., S. H. Woodward, M. Kim, D. B. Taulbee and H. Meng, (2006). Validation of CFD simulations of cerebral aneurysms with implication of geometric variations. *Journal of biomechanical engineering* 128(6), 844–851.

Hu, L. H., Y. Xu, W. Zhu, L. Wu, F. Tang and K. H. Lu (2011). Large eddy simulation of pollutant gas dispersion with buoyancy ejected from building into an urban street canyon. *Journal of Hazardous Materials* 192(3), 940–948.

Karthik, T. S. D. (2011). Turbulence models and their applications. *10th Indo German Winter*

*Academy*, 1–52.

Kashi, E., F. Shahraki, D. Rashtchian and A. Behzadmehr (2009). Effects of vertical temperature gradient on heavy gas dispersion in build up area. *Iranian journal of chemical engineering* 6(3), 26–45.

Kashi, E., F. Mirzaei and F. Mirzaei (2015a). Analysis of gas dispersion and ventilation within a comprehensive CAD model of an offshore platform via computational fluid dynamics. *Journal of Loss Prevention in the Process Industries* 36, 125–133.

Kashi, E., F. Mirzaei and F. Mirzaei (2015b). Analysis of chlorine gas incident simulation and dispersion within a complex and populated urban area via computational fluid dynamics. *Advances in Environmental Technology* 1, 49–58.

Katz, A. and V. Sankaran (2011). Mesh quality effects on the accuracy of CFD solutions on unstructured meshes. *Journal of Computational Physics* 230(20), 7670–7686.

Kim, J. J. and J. J. Baik (2003). Effects of inflow turbulence intensity on flow and pollutant dispersion in an urban street canyon. *Journal of Wind Engineering and Industrial Aerodynamics* 91(3), 309–329.

Li, Y. and T. Stathopoulos (1997). Numerical evaluation of wind-induced dispersion of pollutants around a building. *Journal of Wind Engineering and Industrial Aerodynamics* 67, 757–766.

Lien, F. S., E. Yee, H. Ji, A. Keats and K. J. Hsieh (2006). Progress and challenges in the development of physically-based numerical models for prediction of flow and contaminant dispersion in the urban environment. *International Journal of Computational Fluid Dynamics* 20(5), 323–337.

Mokhtarzadeh-dehghan, M. R., A. Akcayoglu and A. G. Robins (2012). Journal of Wind Engineering Numerical study and comparison with experiment of dispersion of a heavier-than-air gas in a simulated neutral atmospheric boundary layer. *Journal of Wind Engineering and Industrial Aerodynamics* 110, 10–24.

Nakiboğlu, G., C. Gorlé, I. Horváth, J. van Beeck and B. Blocken (2009). Stack gas dispersion measurements with large scale-PIV, aspiration probes and light scattering techniques and comparison with CFD. *Atmospheric environment* 43(21), 3396–3406.

Santiago, J. L., A. Martilli and F. Martilli (2007). CFD simulation of airflow over a regular array of cubes. Part I: Three-dimensional simulation of the flow and validation with wind-tunnel measurements. *Boundary-layer meteorology* 122(3), 609–634.

Sklavounos, S. and F. Rigas (2004). Validation of turbulence models in heavy gas dispersion over obstacles. *Journal of Hazardous Materials* 108, 9–20.].

Tominaga, Y. and L. Guo-cheng (2012). CFD simulations of pollutant gas dispersion with different buoyancies around an isolated building. *In The Seventh International Colloquium on Bluff Body Aerodynamics and Applications (BBAA7)*, 2-6.

Tominaga, Y. and T. Stathopoulos (2013). CFD simulation of near-field pollutant dispersion in the urban environment: A review of current modeling techniques. *Atmospheric Environment* 79, 716–730.

Tominaga, Y. and T. Stathopoulos (2007). Turbulent Schmidt numbers for CFD analysis with various types of flowfield. *Atmospheric Environment* 41(37), 8091–8099.

Vardoulakis, S. and X. Cai (2011). A novel methodology for interpreting air quality measurements from urban streets using CFD modelling 45, 5230–5239.

Wallin, S. and A. V. Johansson (2000). An explicit algebraic Reynolds stress model for incompressible and compressible turbulent flows. *Journal of Fluid Mechanics* 403, 89-132.

Yakhot, V., S. A. Orszag, S. Thangam, T. B. Gatski and C.G. Speziale (1992). Development of turbulence models for shear flows by a double expansion technique. *Physics of Fluids* 4(7), 1510–1520.

Yang, B. and K. M. Zhang (2017). CFD-based turbulent reactive fl ow simulations of power plant plumes. *Atmospheric Environment* 150, 77–86.

Yu, H. and J. The (2016). Validation and optimization of SST k-ω turbulence model for pollutant dispersion within a building array. *Atmospheric Environment* 145, 225–238.

Zhiyin, Y. (2015). Large-eddy simulation: Past, present and the future. *Chinese Journal of Aeronautics* 28(1), 11–24.

Zhu, H., Z. Mao, Q. Wang and J. Sun (2013). The influences of key factors on the consequences following the natural gas leakage from pipeline. *Procedia Engineering* 62, 592–601.